Title
Improving fast-ion confinement in high-performance discharges by suppressing Alfvén eigenmodes

Journal
Nuclear Fusion, 57(5)

ISSN
0029-5515

Authors
Kramer, GJ
Podestà, M
Holcomb, C
et al.

Publication Date
2017-05-01

DOI
10.1088/1741-4326/aa6456

IOP Publishing | International Atomic Energy Agency Nuclear Fusion

Nucl. Fusion **57** (2017) 056024 (7pp) https://doi.org/10.1088/1741-4326/aa6456

Improving fast-ion confinement in high-performance discharges by suppressing Alfvén eigenmodes

G.J. Kramer[1], M. Podestà[1], C. Holcomb[2], L. Cui[1], N.N. Gorelenkov[1], B. Grierson[1], W.W. Heidbrink[3], R. Nazikian[1], W. Solomon[4], M.A. Van Zeeland[4] and Y. Zhu[3]

[1] Princeton Plasma Physics Laboratory, PO Box 451, Princeton, NJ 08543-0451, United States of America
[2] Lawrence Livermore National Laboratory, Livermore, CA 94550, United States of America
[3] University of California Irvine, Irvine, CA 92697, United States of America
[4] General Atomics, PO Box 85608, San Diego, CA 92186-5608, United States of America

E-mail: gkramer@pppl.gov

Received 9 January 2017, revised 14 February 2017
Accepted for publication 3 March 2017
Published 28 March 2017

Abstract

We show that the degradation of fast-ion confinement in steady-state DIII-D discharges is quantitatively consistent with predictions based on the effects of multiple unstable Alfvén eigenmodes on beam-ion transport. Simulation and experiment show that increasing the radius where the magnetic safety factor has its minimum is effective in minimizing beam-ion transport. This is favorable for achieving high performance steady-state operation in DIII-D and future reactors. A comparison between the experiments and a critical gradient model, in which only equilibrium profiles were used to predict the most unstable modes, show that in a number of cases this model reproduces the measured neutron rate well.

Keywords: fast-ion transport, Alfvén eigenmodes, high-performance plasmas

(Some figures may appear in colour only in the online journal)

1. Introduction

Anomalous fast-ion transport has been problematic in DIII-D for reaching a steady-state regime in some types of discharges which are characterized by high values of the normalized pressure, β_N and low-shear q profiles with q_{min} near two [1]. Fast-ion redistribution reduces the neutral-beam current drive (NBCD) and limits the β that can be obtained at fixed beam power. This can make it difficult to drive a sufficient bootstrap current to reach steady state those discharges. Reducing the fast-ion transport down to classical levels will help to achieve non-inductive current-dominated discharges with q_{min} near two.

During the steady-state phase of neutral beam heated DIII-D discharges with high $q_{min}(>2)$ and high poloidal β larger than two [1] a rich spectrum of Alfvén eigenmodes (AEs) is observed on multiple diagnostics such as the CO_2 interferometer as can be seen in figures 1(*a*) and 2(*a*). The AEs appear in the Doppler-shifted toroidicity and ellipticity induced frequency gaps and therefore identified as TAEs and EAEs. When the AEs are present the measured neutron rate can be up to 40% lower than the classically expected neutron rate [2]. The classical neutron rate is based on fast-ion transport due to slowing-down and pitch angle scattering processes and is usually obtained from the TRANSP code [3]. Earlier work has shown that there is a strong correlation between the observed neutron deficit and the integrated mode amplitude in the TAE and EAE frequency range [2] although no causal relation was established. AE-driven fast-ion transport has been modeled with ad-hoc fast-ion diffusion coefficients [4] which were adjusted in the simulations to yield the measured neutron deficits. Although the deduced diffusion coefficients correlated with the observed AE activity, there was no physics-based causal relation between the diffusion coefficients and the AEs in this model.

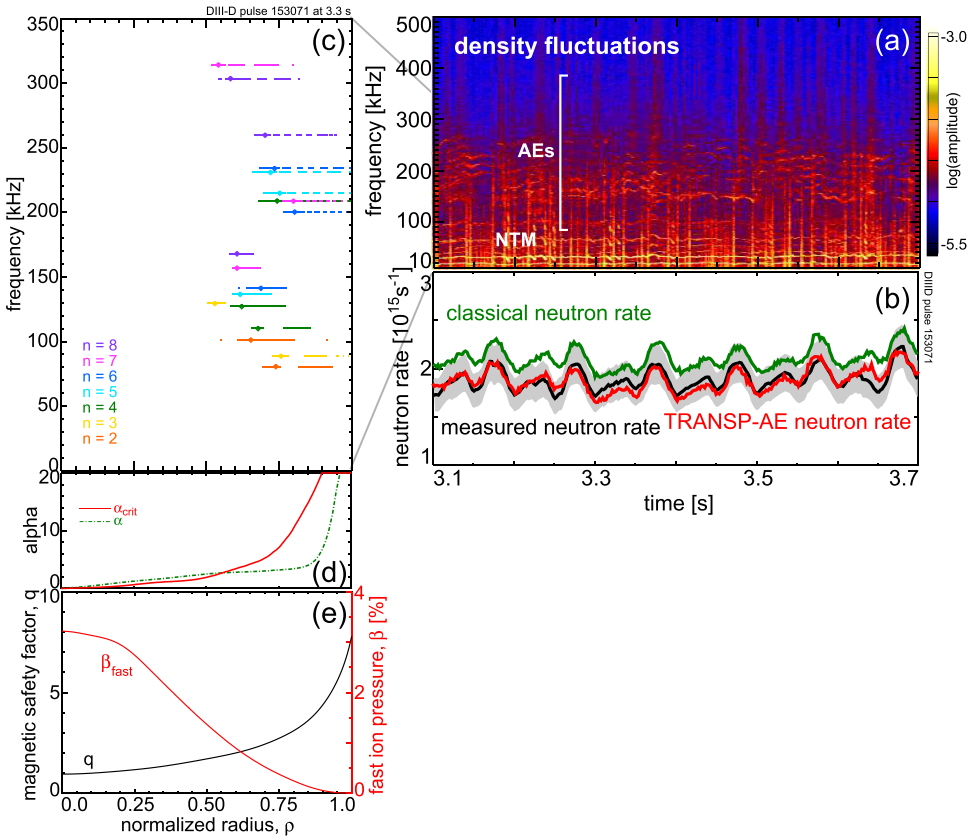

Figure 1. A normal shear high-performance steady-state target discharge (DIII-D pulse 153 071). (*a*) Observed density fluctuations (*b*) measured (black), classical (green) neutron rate and the neutron in which the effects of AEs are included (red). (*c*) NOVA spectrum of TAEs (below 180 kHz) and EAEs (above 180 kHz) used in the calculations. (*d*) Obtained (green) and critical (red) normalized pressure gradients. (*e*) Fast-ion pressure profile (red) and magnetic safety factor profile (black).

We show that the observed neutron deficit in the afore mentioned DIII-D discharges can be fully attributed to the observed AEs (section 2) by comparing the experiments with results from a kick model [5] that takes into account the resonant effects between the AEs and the fast ions via correlated kicks in energy and canonical angular momentum, and therefore, a causal relation can be established between the observed AE activity and the neutron deficit.

Once it is established that the fast-ion transport is driven by AE activity, theoretical models on how to suppress the AE activity by modifying the magnetic safety factor profile are discussed (section 3), and it is investigated experimentally whether the proposed solutions to suppress AE activity can restore the plasma performance as determined from the observed neutron rate.

Because the observed AEs can explain the observed neutron deficit, these discharges were used to test a critical gradient model [6] showing that the measured neutron rates can be reproduced when only equilibrium profiles are given and no measurements of AE activity are avaliable (section 4). A summary and conclusions are presented in the final section (section 5).

2. Fast-ion transport modeling

The kick model which is described in detail in [5] uses the wave-particle resonances in phase space to model the fast-ion transport. The kicks are obtained from correlated changes in energy and canonical angular momentum as calculated by the ORBIT code [7] in which an ensemble of fast-ion test particles is followed using the guiding center approximation. The experimental toroidal geometry and fields are used together with the the mode structures that are obtained from the ideal MHD NOVA code [8, 9]. The kicks are then added to the NUBEAM code [10] which simulates the slowing-down and pitch angle scattering for the fast ions in TRANSP. In the NUBEAM code the fast ions are propagated in phase space between the time steps that are used in the TRANSP code so that the effects of both classical slowing-down and the AEs are included. The mode spectra and amplitudes which are needed as input in this case are all obtained from the experiments and therefore, the kick model is a descriptive model and well suited to investigate whether the observed neutron deficit is solely due to AE-induced fast-ion transport.

When the effects of the AEs on the fast-ion population are included in TRANSP by using the kick model, the calculated neutron rate decreases to the measured one as is shown in figure 1(*b*) for a normal shear high performance steady-state discharge with a modest neutron deficit of 10%. The main plasma parameters for this discharge (number 153 071) were: $I_p = 0.91$ MA, $B_T = 1.8$ T, $\beta_N = 2.6$, $q_0 = 1.0$, $q_{95} = 6.5$, $n_e(0) = 5.7\,10^{19}$ m^{-3}, $T_e(0) = 3.4$ keV, and $T_i(0) = 5.9$ keV.

Similarly, the observed much larger neutron deficit in the reversed shear high performance steady-state discharge as shown in figure 2(*b*) is also reproduced accurately by the kick model despite the presence of a neo-classical tearing mode (NTM). The

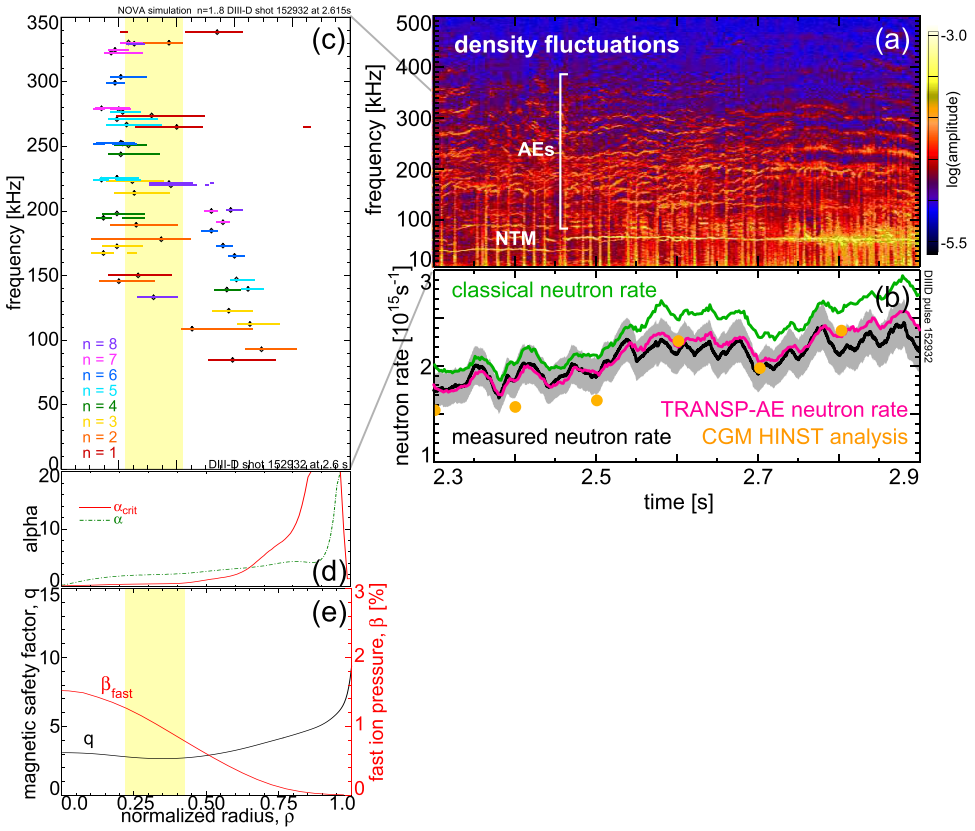

Figure 2. A reversed shear high-performance steady-state target discharge (DIII-D pulse 152932). (*a*) Observed density fluctuations (*b*) measured (black), classical (green) neutron rate and the neutron in which the effects of AEs are included (red) while the dots (yellow) show the results of a critical gradient model analysis. (*c*) NOVA spectrum of RSAEs and TAEs used in the calculations. (*d*) Obtained (green) and critical (red) normalized pressure gradients. (*e*) Fast-ion pressure profile (red) and magnetic safety factor profile (black). The yellow bands in (*c*) and (*e*) indicate the low shear region near $q_{\min}$.

NTM was not included in the kick model analysis because the NTM amplitude was below the threshold for field-line stochasticity and therefore, the fast-ion transport is hardly affected by NTM activity as was shown in [11]. At much larger NTM amplitudes than observed in this experiment, however, NTMs can induce significant fast-ion transport [12]. The main plasma parameters for this discharge (number 152932) were: $I_p = 0.95\,\mathrm{MA}$, $B_T = 2.0\,\mathrm{T}$, $\beta_N = 2.6$, $q_0 = 3.0$, $q_{\min} = 2.4$, $q_{95} = 5.6$, $n_e(0) = 4.5\,10^{19}\ \mathrm{m}^{-3}$, $T_e(0) = 3.7\,\mathrm{keV}$, and $T_i(0) = 6.2\,\mathrm{keV}$.

This agreement between the measurements and the kick model results indicates that the observed neutron deficiency can fully be attributed to AE-driven fast-ion transport. With this finding we will investigate two important topics: (1) how to suppress the AE activity as much as possible and improve the plasma performance in steady-state target plasmas and (2) benchmark a critical gradient model so that it can be used for fast-ion transport predictions from equilibrium profiles only without the experimental knowledge of the Alfvén eigenmode spectrum. After a successful benchmark, the critical gradient may then be applied to fast-ion transport and plasma performance studies for ITER.

3. Alfvén eigenmode suppression techniques

Two conditions have to be met for the excitation of AEs in plasmas: first, the eigenmode has to exist in the plasma and, second, the mode has to be driven unstable, usually via wave-particle interactions between the Alfvén eigenmodes and the fast ions. This leads to two methods for suppressing AEs in fusion plasmas: (1) the eigenmodes can be pushed out of their gaps and into the Alfvén continuum by manipulating the equilibrium profiles, (2) the fast-ion drive can be changed by moving the fast-ion drive away from the mode location.

The condition under which AEs can exist has been investigated theoretically for modes in the TAE gap [13] and it was found that when the normalized pressure gradient:

$$\alpha = -2\frac{R_0 q(r)^2}{B^2}\frac{\mathrm{d}P(r)}{\mathrm{d}r} \qquad (1)$$

which is proportional to the product of the plasma pressure gradient and the magnetic curvature (R_0 the major radius, B the magnetic field strength, $q(r)$ the magnetic safety factor, and $P(r)$ the plasma pressure profile) exceeds a critical value, α_{crit}, the TAE disappears into the Alfvén continuum. The critical α is given for normally observed TAEs with both poloidal components in phase at the low-field side (a.k.a. even TAEs) as $\alpha_{\mathrm{crit}} \approx 3\epsilon + 2s^2$ with ϵ the inverse aspect ratio and $s = r/q\ \mathrm{d}q/\mathrm{d}r$ the magnetic shear. It was found that the existence and suppression of TAEs agreed well with observed TAE behavior as was shown in [14] for even TAEs and for odd TAEs in [15]. (Odd TAE have a 180 deg. phase shift between the poloidal harmonics at the low-field side). Therefore, by increasing α, the core TAEs can be suppressed as illustrated

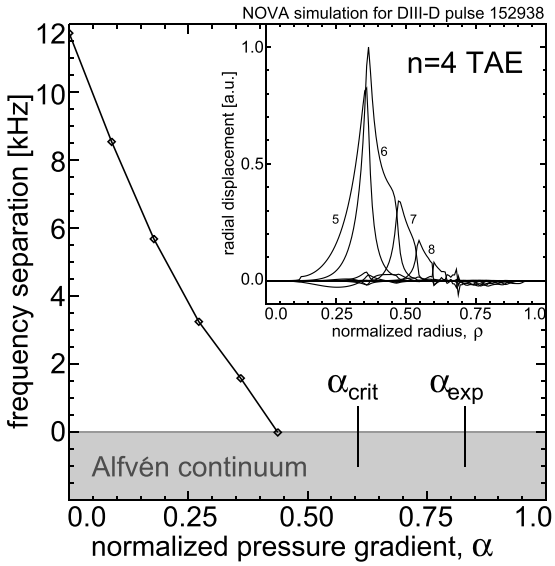

Figure 3. The $n = 4$ TAE (inset) disappears into the Alfvén continuum when the normalized pressure gradient passes a threshold. Solid line: NOVA simulation, $\alpha_{\rm crit}$ high-n ballooning prediction, $\alpha_{\rm exp}$ the experimentally obtained value. The frequency separation is the difference between the TAE frequency and the top of the Alfvén continuum at the mode location.

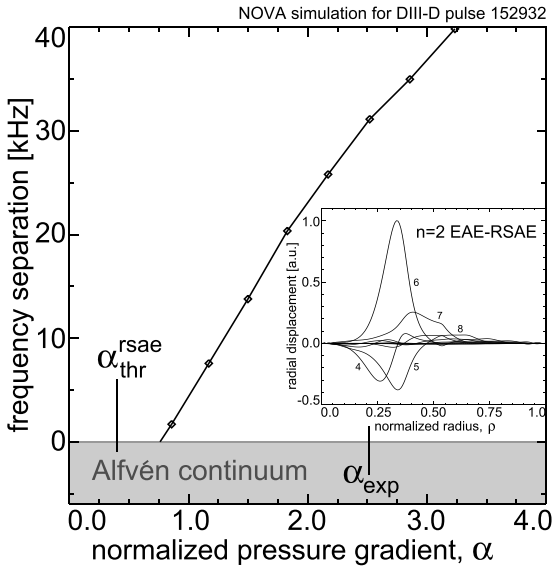

Figure 4. The $n = 2$ RSAE associated with the EAE gap (inset) emerges from the Alfvén continuum when the normalized pressure gradient passes a threshold. Solid line: NOVA simulation, $\alpha_{\rm thr}$ high-n ballooning prediction, $\alpha_{\rm exp}$ the experimentally obtained value. The frequency separation is the difference between the TAE frequency and the top of the Alfvén continuum at the mode location.

in figure 3. When α is increased in NOVA simulations the frequency separation between the TAE frequency and the frequency at the top of the Alfvén continuum where the mode is located decreases until the TAE frequency reaches the continuum frequency and the TAE disappears into the continuum. In the NOVA simulations the TAE disappears into the Alfvén continuum at a slightly lower value of α than the $\alpha_{\rm crit}$ predicted by analytical theory which can be attributed to approximations that were made in the analytic calculation [13]. In high-performance discharges the critical α value is routinely exceeded in the plasma center and core-localized TAEs are suppressed.

A good example of TAE suppression via this mechanism is shown in figure 1(c) for the normal shear discharge. No TAEs were found inside $\rho < 0.5$ which coincides with the region where $\alpha > \alpha_{\rm crit}$ as shown in figure 1(d) despite that the fast ion pressure (figure 1(e)) has a steep gradient in that region which can potentially drive strong AE activity as was found in the plasma core for the reversed shear case (figures 2(c)–(e)).

Increasing α can be achieved by increasing the pressure gradient but increasing the pressure gradient will destabilize MHD activity such as tearing modes [16] and hence degrade the plasma performance. A better way to increase α is by raising q_0 and elevating the q profile in the plasma center. Note that α is proportional to q^2, so raising q_0 is an effective way to increase α while $\alpha_{\rm crit}$ depends on the shear and is independent of q_0.

Although TAE activity can be suppressed by moving α above the critical value for suppression, Reversed Shear Alfvén Eigenmodes (RSAEs) behave in the opposite way: they emerge from the Alfvén continuum when α increases and establish themselves in the AE gaps virtually undamped as was found theoretically [17] and experimentally [18]. When α increases, the RSAEs associated with the TAE gap move away from the Alfvén continuum into the TAE gap as was studied experimentally in [19] while the RSAEs associated with the EAE, NAE (Noncircular triangularity-induced AE), and higher order gaps emerge from the Alfvén continuum as is shown in figure 4 for an EAE-RSAE.

An analytic criterion for the existence of RSAEs associated with the TAE gap near the shear reversal point was derived in [20] where a 'Schrödinger potential well', Q, was used in the RSAE wave equation. It was found that when Q was larger than 1/4, RSAE solutions do exist and an explicit expression for Q was given in [20] that depends on local geometry and plasma parameters near $q_{\rm min}$. In later work Q has been calculated with additional assumptions for the plasma and/or contributions from the fast-ions [21, 22]. In [17] Q was calculated for RSAEs associated with the EAE, NAE, and higher order gaps and it was found that Q is positive for TAE–RSAEs while for the EAE-, NAE-, and higher order RSAEs there is a threshold in α which is given in the high poloidal mode number limit as:

$$\alpha_{\rm thr} = (b + \sqrt{b^2 + 3}\,)\epsilon \qquad (2)$$

with $b = 1 + 2(1 - q_{\rm min}^{-2})((2k_m q_{\rm min})^{-2} - 1)$ above which the RSAEs come into existence ($q_{\rm min}$ value of q at the shear reversal point and $k_m = n - m/q_{\rm min}$). For finite poloidal mode numbers equation (2) is modified slightly and $\alpha_{\rm thr}$ is dependent on the major radius and the shear rate near $q_{\rm min}$ as was shown in [17].

Therefore, increasing α, which was favorable to suppress TAE activity, is destabilizing for RSAE activity and some other way has to be devised to reduce the RSAE activity for better plasma performance. An obvious way to eliminate the RSAEs is to operate the plasma with a monotonic q profile and eliminate the shear reversal point where the RSAEs are

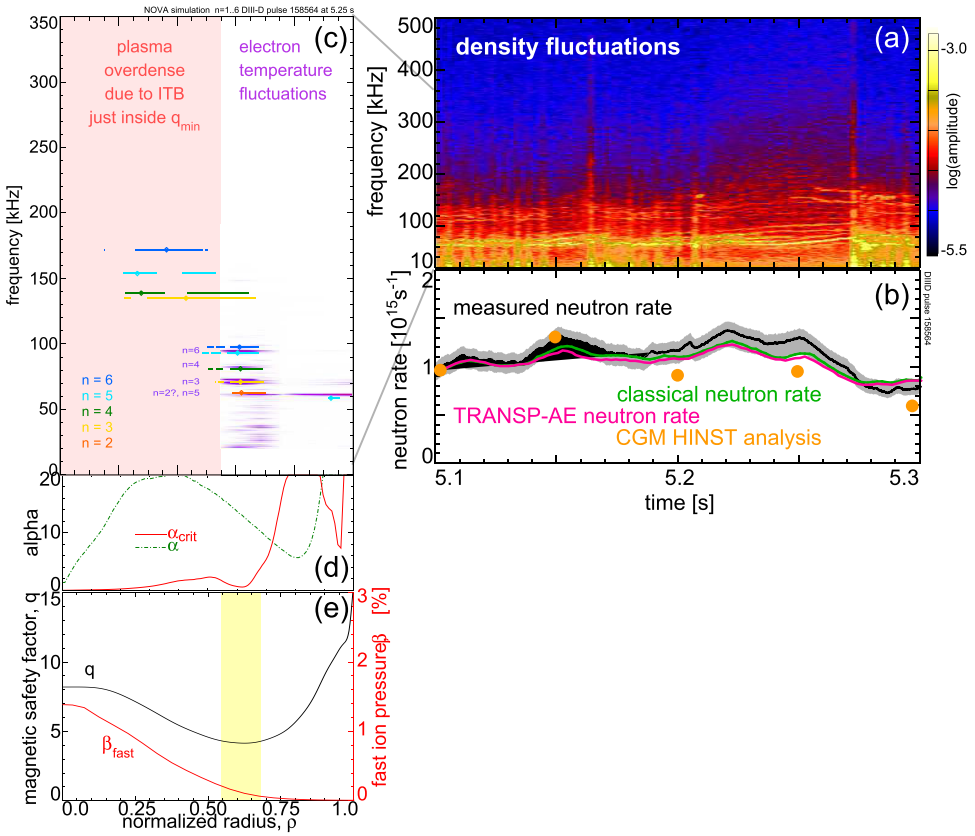

Figure 5. A high $\beta_{\rm pol}$ reversed shear discharge (DIII-D pulse 158 564). (*a*) Observed density fluctuations (*b*) measured (black), classical (green) neutron rate and the neutron in which the effects of AEs are included (red) while the dots (yellow) show the results of a critical gradient model analysis. (*c*) NOVA spectrum of modes used in the calculations overlayed on the radially resolved ECE spectrum measured outside $\rho = 0.55$. (*d*) Obtained (green) and critical (red) normalized pressure gradients. (*e*) Fast-ion pressure profile (red) and magnetic safety factor profile (black). The yellow band in (*c*) indicates the low shear region near $q_{\rm min}$.

located as was done for discharge 153 071 shown in figure 1. This, however, might not be the best option for steady state plasma operation, in which a broad pressure profile is used to induce a significant bootstrap current to help sustain the non-inductive plasma current.

A better way to suppress RSAEs is to reduce the fast-ion drive as much as possible at the location of $q_{\rm min}$. This was achieved in DIII-D by moving $q_{\rm min}$ outward and away from the steep fast-ion pressure gradient region as was done in discharge 158 564 and shown in figure 5(*e*). In this discharge the following plasma parameters were obtained: $I_{\rm p} = 0.69$ MA, $B_{\rm T} = 2.0$ T, $\beta_p = 3.4$, $q_0 = 8.2$, $q_{\rm min} = 3.8$, $q_{95} = 11.9$, $\mathrm{n(0)}_e = 6.5\,10^{19}\,\mathrm{m}^{-3}$, $T_e(0) = 2.5$ keV, $T_i(0) = 3.5$ keV.

The position of $q_{\rm min}$ was located at $\rho = 0.65$ (figure 5(*e*)) and was established there by using all the available off-axis current drive in DIII-D and reducing the plasma current from 1 MA in normal high-performance steady state discharges to 0.7 MA thereby creating a high β_p discharge. For this type of discharge, the non-inductive current drive (ECCD and NBI) was sufficient to sustain an off-axis current profile with a large $q_{\rm min}$ radius. The strongest AE activity is measured between 50 and 100 kHz and is located near $q_{\rm min}$ and NOVA simulations show that these modes are RSAEs. Above 100 kHz some mode activity is sometimes (around 5.26 s) visible in the density fluctuation spectrum (figure 5(*a*)) that does not appear outside $\rho = 0.55$ in the ECE spectra (figure 5(*c*)). The plasma was overdense inside $\rho = 0.55$ because of an internal transport barrier just inside $q_{\rm min}$. Although not conclusive, these high frequency modes were found to be compatible with EAEs near the top of the EAE gap as found in NOVA simulations.

Despite the appearance of possible weak EAE activity, this q profile is good for suppressing the normal shear Alfvén activity in the core because α well above $\alpha_{\rm crit}$ (figure 5(*d*)) so that the TAE activity is strongly suppressed.

In this discharge the measured neutron rate matches the classically expected one (figure 5(*b*)) within the error bars while the inclusion of the AEs in the TRANSP simulation does not change the simulated neutron rate because the fast-ion drive for the RSAEs is much weaker at this large radius compared to the case where $q_{\rm min}$ is located around $\rho = 0.3$ as was the case in pulse 152 932 (figure 2(*e*)). The uncertainty in the calculated neutron rates was estimated to be ten percent due to uncertainties in the experimental inputs used in TRANSP but the difference between the classical and TRANSP-AE neutron rates was not affected by these uncertainties. The remaining benign RSAE activity is very useful to accurately diagnose the location and value of $q_{\rm min}$ which are key parameters for reliable reversed shear equilibrium reconstructions. Information on the q profile from AE spectroscopic techniques are can very valuable [23] especially when other q profile diagnostics such as the motional Stark effect (MSE) diagnostic are not available.

Achieving a similar q profile in high-performance steady state discharges with a 1 MA plasma current requires a stronger off-axis current drive than is currently possible on DIII-D.

4. Critical gradient model analysis

In the DIII-D discharges studied in this paper the fast-ion transport was found to be driven mainly by the observed AEs. Therefore, these discharges are good subjects for benchmarking critical gradient models so that these models can be applied to study and predict the plasma performance in ITER.

Experimentally, fast-ion transport by AEs in DIII-D increases rapidly when the fast-ion gradient exceeds a critical threshold [24–26]. The experimental threshold for appreciable transport occurs when overlapping resonances cause stochastic fast-ion orbits [25]. In simulations where the background plasma is described with a resistive MHD model and the fast ions are treated kinetically, the observed plasma behavior is successfully reproduced [27] but these simulations are computationally intensive. A much simpler theoretical model utilizes a high-n model [28] to calculate local linear AE stability. When the used fast-ion pressure gradient exceeds the calculated threshold, the fast ions are redistributed to match the critical gradient, assuming infinitely stiff transport [29, 30]. In another critical gradient model [31], the threshold occurs when the growth rate of the AEs exceeds the growth rate associated with microturbulence.

The critical gradient model that uses the linear stability threshold [30] was applied to the two reversed shear discharges (figures 2 and 5) with eigenmodes that were obtained from the high-n stability HINST code [32]. In the HINST code a Fourier-ballooning formalism is used to calculate AEs while non-ideal effects are included in a non-perturbative way [28]. The critical gradient model analysis was performed at a number of time points and the neutron rate was calculated from the relaxed fast-ion pressure profiles. The predictions are consistent with the measured neutron rates for half of the calculated time points but underpredict the measured rates for the other times (figures 2(b) and 5(b)). Since appreciable fast-ion transport does not occur until the drive significantly exceeds the linear stability threshold, the tendency to underpredict the neutron rate is expected. Nevertheless, this relatively simple model is useful in providing a pessimistic prediction based solely on equilibrium profiles without any free parameters.

5. Discussion and conclusion

In this paper we have shown that the observed neutron rate deficiency in steady-state target discharges in DIII-D can be attributed to the observed sea of Alfvén eigenmodes as was suggested by a correlation between AE amplitudes and neutron rate deficiencies [2, 4]. This result was obtained from a detailed transport analysis with the TRANSP code in which the effects of the AEs on the fast ions were taken into account via resonant kicks in energy and toroidal canonical momentum [5]. The experimental data were also used to test a critical gradient model that utilizes the linear stability threshold. The model's predictions successfully track the measured neutron rate but tend to underpredict the actual value.

AE-induced fast-ion transport reduces the plasma performance in the steady-state target discharges so suppressing the AE activity and mitigating their adverse effects on the fast-ion confinement is paramount to improve the plasma performance. In this paper, a model that was developed to explain observed core-localized TAEs, was used to guide the experiments to suppress TAE activity in the plasma core by raising the normalized pressure gradient above a critical value where the TAEs are driven into the Alfvén continuum. The most efficient way to increase the normalized pressure gradient is to raise the magnetic safety factor at the magnetic axis.

Although increasing the normalized pressure gradient is very efficient to suppress TAEs, the reversed shear Alfvén eigenmodes become more unstable and RSAEs in higher order gaps come into existence. In this paper it was shown that the RSAEs can be suppressed effectively by moving the shear reversal point away from the steep fast-ion pressure gradient region so that the fast-ion drive for the modes is reduced.

Experimental evidence was presented that when the radius of $q_{\min}$ was moved outward the AE activity was strongly reduced and the classical neutron rates were recovered albeit in a discharge with reduced plasma current.

While conditions for AE suppression have been demonstrated at high $q_{\min}$, a challenge remains to create and sustain high-performance high-current reversed shear discharges in which $q_{\min}$ is located at a sufficiently large minor radius so that the AEs are suppressed. Upgrades to DIII-D are planned with additional off-axis beams and increased electron cyclotron current drive that are expected to increase the radius of $q_{\min}$ and test steady-state solutions for future fusion reactors.

Acknowledgments

This work was supported by the US Department of Energy under DE-AC02-09CH11466, DE-AC52-07NA27344, DE-FC02-04ER54698, and SC-G903402. DIII-D data shown in this paper can be obtained in digital format by following the links at: https://fusion.gat.com/global/D3D_DMP.

References

[1] Holcomb C.T. *et al* 2015 *Phys. Plasmas* **22** 055904
[2] Heidbrink W.W. *et al* 2014 *Plasma Phys. Control. Fusion* **56** 095030
[3] Budny R.V. *et al* 1995 *Nucl. Fusion* **35** 1497
[4] Van Zeeland M.A. *et al*, DIII-D and ASDEX Upgrade Teams 2011 *Phys. Plasmas* **18** 056114
[5] Podestà M., Gorelenkova M. and White R.B. 2014 *Plasma Phys. Control. Fusion* **56** 055003
[6] Gorelenkov N.N., Berk H.L. and Budny R.V. 2005 *Nucl. Fusion* **45** 226
[7] White R.B. and Chance M. 1984 *Phys. Fluids* **27** 2455
[8] Cheng C.Z. and Chance M. 1987 *J. Comput. Phys.* **71** 124
[9] Cheng C.Z. 1992 *Phys. Rep.* **211** 1
[10] Pankin A., McCune D., Andre R., Bateman G. and Kritz A. 2004 *Comput. Phys. Commun.* **159** 157

[11] Heidbrink W.W., Austin M.E., Collins C.S., Gray T., Grierson B.A., Kramer G.J., Lanctot M., Pace D.C., Van Zeeland M.A. and Mclean A.G. 2015 *Nucl. Fusion* **55** 083023
[12] Carolipio E.M., Heidbrink W.W., Forest C.B. and White R.B. 2002 *Nucl. Fusion* **42** 853
[13] Fu G.Y. 1995 *Phys. Plasmas* **2** 1029
[14] Fu G.Y., Cheng C.Z., Budny R., Chang Z., Darrow D.S., Fredrickson E., Mazzucato E., Nazikian R., Wong K.L. and Zweben S. 1996 *Phys. Plasmas* **3** 4036
[15] Kramer G.J., Sharapov S.E., Nazikian R., Gorelenkov N.N. and Budny R.V. 2004 *Phys. Rev. Lett.* **92** 015001
[16] Turco F. *et al* 2012 *Phys. Plasmas* **19** 032506
[17] Kramer G.J. and Fu G.Y. 2006 *Plasma Phys. Control. Fusion* **48** 1285
[18] Kramer G.J., Fu G.Y., Nazikian R., Budny R.V., Cheng C.Z., Gorelenkov N.N., Pinches S.D., Sharapov S.E., Zastrow K.-D. and JET EFDA Contributors 2008 *Plasma Phys. Control. Fusion* **50** 082001
[19] Van Zeeland M.A. *et al* 2016 *Nucl. Fusion* **56** 112007
[20] Berk H.L., Borba D.N., Breizman B.N., Pinches S.D. and Sharapov S. 2001 *Phys. Rev. Lett.* **87** 185002
[21] Breizman B.N., Pekker M.S., Sharapov S.E. and JET EFDA Contributors 2005 *Phys. Plasmas* **12** 112506
[22] Fu G.Y. and Berk H.L. 2006 *Phys. Plasmas* **13** 052502
[23] Kramer G.J., Cheng C.Z., Kusama Y., Nazikian R., Takeji S. and Tobita K. 2001 *Nucl. Fusion* **41** 1135
[24] Heidbrink W.W., Van Zeeland M.A., Austin M.E., Bass E.M., Ghantous K., Gorelenkov N.N., Grierson B.A., Spong D.A. and Tobias B.J. 2013 *Nucl. Fusion* **53** 093006
[25] Collins C.S., Heidbrink W.W., Austin M.E., Kramer G.J., Pace D.C., Petty C.C., Stagner L., Van Zeeland M.A., White R.B., Zhu Y.B. and DIII-D Team 2016 *Phys. Rev. Lett.* **116** 095001
[26] Heidbrink W.W. *et al* 2017 *Phys. Plasma.* **24** 056109
[27] Todo Y., Van Zeeland M.A. and Heidbrink W.W. 2016 *Nucl. Fusion* **56** 112008
[28] Gorelenkov N.N., Cheng C.Z. and Tang W.M. 1998 *Phys. Plasma* **5** 3389
[29] Ghantous K., Gorelenkov N.N., Berk H.L., Heidbrink W.W. and Van Zeeland M.A. 2012 *Phys. Plasmas* **19** 092511
[30] Gorelenkov N.N., Heidbrink W.W., Kramer G.J., Lestz J.B., Podestà M., Van Zeeland M.A. and White R.B. 2016 *Nucl. Fusion* **56** 112015
[31] Waltz R.E., Bass E.M., Heidbrink W.W. and Van Zeeland M.A. 2015 *Nucl. Fusion* **55** 123012
[32] Cheng C.Z. and Gorelenkov N.N. 2004 *Phys. Plasmas* **11** 4784